

GiT: Graph Interactive Transformer for Vehicle Re-identification

Fei Shen, Yi Xie, Jianqing Zhu, Xiaobin Zhu, and Huanqiang Zeng

Abstract—Transformers are more and more popular in computer vision, which treat an image as a sequence of patches and learn robust global features from the sequence. However, a suitable vehicle re-identification method should consider both robust global features and discriminative local features. In this paper, we propose a graph interactive transformer (GiT) for vehicle re-identification. On the whole, we stack multiple GiT blocks to build a competitive vehicle re-identification model, in where each GiT block employs a novel local correlation graph (LCG) module to extract discriminative local features within patches and uses a transformer layer to extract robust global features among patches. In detail, in the current GiT block, the LCG module learns local features from local and global features resulting from the LCG module and transformer layer of the previous GiT block. Similarly, the transformer layer learns global features from the global features generated by the transformer layer of the previous GiT block and the new local features outputted via the LCG module of the current GiT block. Therefore, LCG modules and transformer layers are in a coupled status, bringing effective cooperation between local and global features. This is the first work to combine graphs and transformers for vehicle re-identification to the best of our knowledge. Extensive experiments on three large-scale vehicle re-identification datasets demonstrate that our method is superior to state-of-the-art approaches. The code will be available soon.

Index Terms—Deep Learning, Graph Network, Spatial Significance, Vehicle Re-identification

I. INTRODUCTION

Vehicle re-identification [1, 2] aiming to retrieve a target vehicle from non-overlapping cameras has attracted much attention in the multimedia and computer vision community. With the widespread use of intelligent video surveillance systems, the demand for vehicle re-identification is growing exponentially. However, vehicle re-identification is challenging. Since vehicle images of different identifications usually have similar global appearances and subtle differences in local regions (e.g., wheels, lights, and front windows.) Therefore,

This work was supported in part by the National Natural Science Foundation of China under the Grants 61976098, 61871434, 61802136 and 61876178, in part by the National Key R&D Program of China under the Grant of 2018YFB0803700, in part by the Natural Science Foundation for Outstanding Young Scholars of Fujian Province under the Grant 2019J06017, in part by the Key Science and Technology Project of Xiamen City under the Grant 3502ZCQ20191005, in part by the Science and Technology Bureau of Quanzhou under the Grant 2018C115R, and in part by the Postgraduates' Innovative Fund in Scientific Research of Huaqiao University under the Grant 18014084008. (Corresponding author: Jianqing Zhu and Huanqiang Zeng).

Fei Shen, Yi Xie, Jianqing Zhu and Huanqiang Zeng are with College of Engineering, Huaqiao University, Quanzhou, 362021, China (e-mail: {fshen and yixie}@stu.hqu.edu.cn, e-mail: {jqzhu and zeng0043}@hqu.edu.cn).

Xiaobin Zhu is School of Computer and Communication Engineering, University of Science and Technology Beijing, Xueyuan Road 30, Haidian District, Beijing, 100083 China (e-mail: zhuxiaobin@ustb.edu.cn).

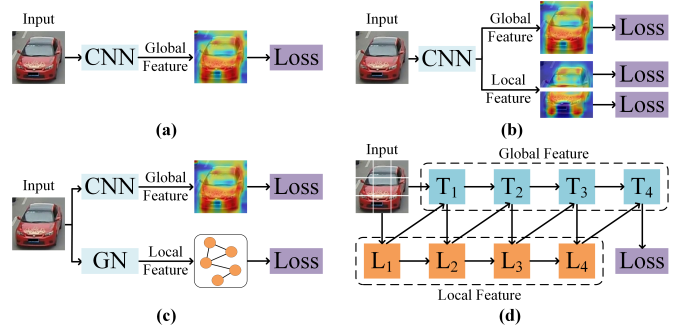


Fig. 1. Vehicle re-identification models using different architectures. (a) Pure convolutional neural networks (CNN) learn global features. (b) Pure convolutional neural networks (CNN) cooperate part divisions to learn global features and local features. (c) CNNs cooperate graph networks (GN) to learn global features and local features. (d) Our method couples global features and local features via transformer (T) layers and local (L) correlation graph modules.

effectively combining the global features and local features is crucial to improve the vehicle re-identification performance.

The development of vehicle re-identification technologies goes through three stages. As shown in Figure 1 (a), early methods [3–7] apply pure convolutional neural networks (CNNs) to learn the vehicle images’ global features. The architectures of these pure CNNs consist of a famous backbone network (such as VGGNet [8], GoogLeNet [9] and ResNet [10]) and a global pooling layer. Although early methods can learn global appearance features, they could not deal with local features, limiting the vehicle re-identification performance.

Vehicle re-identification methods enter into the second stage, which focuses on addressing global features’ limitations. As shown in Figure 1 (b), based on CNNs, there is a straightforward way of combining global features and local features learned from vehicle image partitions. The partition division way can be further summarized into two kinds, i.e., uniform spatial division methods [3, 11–17] and part detection methods [7, 18–23]. The uniform spatial division methods do not require part annotations but are prone to suffer from partition misalignments. In contrast, the part detection methods can relieve dis-alignments but encounter a high cost of extra manual part annotations and massive training computations. No matter how to divide partitions, the subsequent feature learning is individually implemented on each part region, ignoring relationships among part regions.

Third, to consider relationships among part regions, vehicle re-identification methods enter the third stage, combining graph network (GN) with CNNs. As shown in Figure 1 (c),

in this stage, vehicle re-identification models [24–27] usually have a CNN branch for learning global features and a GN branch for exploring the relationship among local features extract from part regions. However, first, the CNN’s down-sampling and convolution operations reduce the resolution of feature maps, greatly affecting the ability to recognize vehicle with similar appearances [28, 29]. Second, the CNN and graph network branches are supervised with two independent loss functions and lack interaction, restricting vehicle re-identification performance.

Recently, the transformer-based models [28–31] are more and more popular in computer vision. Compared with the CNN model, the transformer-based model is more suitable for learning global features for the following reasons. (1) The transformer can use multi-head attention module to capture global context information to establish long-distance dependence on global features of vehicles. (2) The multi-head attention module of transformer does not require convolution and down-sampling operations, which retain more detailed vehicle information. The advantages of extracting global features motivate us to introduce pure transformers for vehicle re-identification. However, the transformer-based model still lacks an effective mechanism to learn discriminative local features. Another problem is that, how to effectively use robust global features and discriminative local features for vehicle re-identification.

This paper first proposes an effective mechanism to learn the local features of the vehicle and then explores an effective feature learning way that considers the relationship between global features and local features. As shown in Figure 1 (d), we propose a graph interactive transformer (GiT) method to couple with global features and local features to improve vehicle re-identification performance. On the whole, we stack multiple GiT blocks to build a competitive vehicle re-identification model. Each GiT block employs a novel local correlation graph (LCG) module to extract discriminative local features within patches and use a transformer layer to obtain robust global features among the patches. In detail, in the current GiT block, the LCG module learns local features from local and global features resulting from the LCG module and transformer layer of the previous GiT block. Similarly, the transformer layer learns global features from the global features generated by the transformer layer of the previous GiT block and the new local features outputted via the LCG module of the current GiT block. Therefore, LCG modules and transformer layers are in a coupled status, bringing effective cooperation between local and global features.

The main contributions of this paper can be summarized as follows:

- We design a local correlation graph (LCG) module for learning discriminative local features within patches via part regions’ relationships. The LCG module does not require any extra fine-grained part annotations or part division operations.
- We propose a graph interactive transformer (GiT) method to couple LCG modules and transformer layers, bringing effective cooperation between local and global features. This paper is the first work that explores the interaction

between local features and global features via graphs and transformers to the best of our knowledge.

- Experiment results on three large-scale vehicle datasets (i.e., VeRi776 [32], VehicleID [33], and VeRi-Wild [34]) show that the proposed method is superior to a lot of state-of-the-art vehicle re-identification approaches.

The rest of this paper is organized as follows. Section II introduces the related work. Section III elaborates our method. Section IV presents the experimental results to show our method’s superiority. Section V concludes this paper.

II. RELATED WORK

In this section, we briefly review the most related works of vehicle re-identification and transformer in vision.

A. Vehicle Re-identification

Since the convolutional neural network (CNN) was proposed, it has extensively promoted vehicle re-identification development. Therefore, we review the CNN models of vehicle re-identification from the following two aspects: (1) pure CNN-based methods (2) combining CNN with graph network.

Pure CNN-based methods. In recent years, a variety of pure CNN-based methods have been proposed for vehicle re-identification. These methods usually include a robust CNN model for extract global features or local features and a feature aggregation structure for aggregate global features or local features. According to the difference in feature aggregation structure, we can subdivide it into global feature learning methods and local feature learning methods. The global feature learning methods [2, 5, 21, 33, 35–46] usually have a spatial global pooling layer to compress the entire vehicle features. However, due to the characteristic of spatial global pooling layers, discriminative local features will inevitably be underestimated, which is detrimental to vehicle re-identification.

According to the local feature learning methods, we can further summarize it as uniform spatial division [3, 11–17] and part detection methods [7, 18–23]. The uniform spatial division methods uniformly divide feature maps into several parts and then individually pools each region, as done in [11–13]. There is also a method of using a visual attention model to refine local features in [15–17]. However, due to vehicle appearance differences and camera viewing angle changes, these methods will face the problem of not accurately dividing the parts, limiting the performance of vehicle re-identification.

The part detection methods can satisfactorily resolve the problem of part dis-alignment. These methods usually employ the typical detectors to detect vehicle parts or locate discriminative regions in [7, 18–23]. For example, the Part Regularization [18] method uses you only look once (YOLO) [47] as a detector to detect parts and feature extraction from part regions. However, the detectors are deep networks in themselves, requiring a high cost of the extra manual part annotations, massive training, and inference computations. Moreover, no matter how the partition is divided or located, the subsequent feature extraction is individually implemented on each part region, ignoring relationships among the part region.

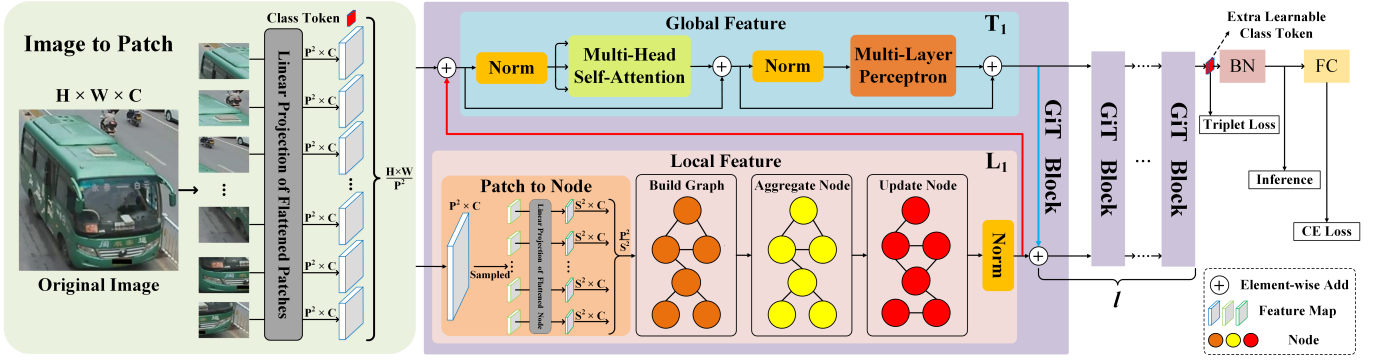


Fig. 2. The framework of the proposed graph interactive transformer (GiT) method. The T and L denote a transformer layer and a local correlation graph (LCG) module. The BN and FC represent a batch normalization and a fully connected layer, respectively.

Combining CNN with Graph Network. Recently, various research efforts [24–27, 48, 49] combine CNN with graph network (GN) based reasoning for re-identification since GN can extract the regional/node feature of the graph structure. For example, the parsing-guided cross-part reasoning network (PCRNet)[24] extracted regional features for each part from CNN and propagated local information among parts based on graph convolutional networks. Wang *et al.* [50] constructed a global structure graph from the features generated by the CNN and guidance to produce effective representations of vehicles. The structured graph attention network (SGAT) [26] created an inherently structured graph and an extrinsic structured graph to learn the vehicle’s structure relationship feature. Besides, the hierarchical spatial structural graph convolutional network (HSS-GCN) [25] enhanced the spatial geometrical structure relationship among local regions or between the global region and local regions for vehicle re-identification. Even though these methods consider relationships between local regions, they ignore the relationship between global and local features, restricting vehicle re-identification performance.

B. Transformer in Vision

The transformer is a type of self-attention-based neural network originally applied for natural language modeling (NLP) tasks. Recently, attention-based transformers have gone viral in vision. The vision transformer (ViT) [28] stacks multiple transformer layers. Every transformer layer is a kind of residual structure. It is sequence packaged by layer normalization (LN), multi-head self-attention layer (MHSA) and a multilayer perceptron (MLP) block. Based on the ViT models, many excellent networks are developed and verified for their effectiveness and scalability in downstream tasks. For example, ViT-BoT [29] combines the ViT framework with BNNeck [51] to construct a strong baseline for object re-identification. Deformable transformer (DETR) [30] proposes multi-scale deformable attention modules to sample a set of critical points of patch for small objects detection. TransUNet [31] takes the advantages of the CNN and transformer model to learn global context features for medical image segmentation.

Considering the strong ability of the graph network to aggregate local features and the superiority of the ViT model

to model global features, we design a novel architecture to graph network and transformer layers are in a coupled status and demonstrate its effectiveness in this paper.

III. PROPOSED METHOD

A. Overview

A suitable vehicle re-identification method should consider both robust global features and discriminative local features, as discussed in previous sections. This paper proposes a graph interactive transformer (GiT) method for the vehicle re-identification method to simultaneously learn global features and local features, as shown in Figure 2. In our framework, the GiT method consists of multiple GiT blocks. Each GiT block employs a novel local correlation graph (LCG) module to extract discriminative local features within patches and uses a transformer layer to extract robust global features among patches. Moreover, LCG modules and transformer layers are in a coupled status, bringing effective cooperation between local and global features. More detail about the GiT method and loss functions are described as follows.

B. Local Correlation Graph Module

We propose a local correlation graph (LCG) module to aggregate and learn discriminative local features within every patch. Assume each vehicle image have N patches and the i -th patch $N_i = P^2 \times C$, where P^2 and C respectively denote the patch’s size and the number of channels. In the LCG module, each patch is sampled into n local features of a sequence of (S, S) size with d dimensions features, where $n = \frac{P^2}{S^2}$ and $d = S^2 \times C$. Like patch embedding of ViT, we flatten n local features d dimensions and map to d' dimensions with a trainable linear projection in every patch. The transformed local feature sequence of i -th patch is formed according to Eq. (1) as follows:

$$X_i = [x_i^1 E, x_i^2 E, \dots, x_i^m E, \dots, x_i^n E], \quad (1)$$

where $X_i \in \mathbb{R}^{n \times d'}$ and $E \in \mathbb{R}^{d \times d'}$. Then, we create a learnable position embedding E_{pos} to preserve the position information for each local feature, where $E_{pos} \in \mathbb{R}^{n \times d'}$.

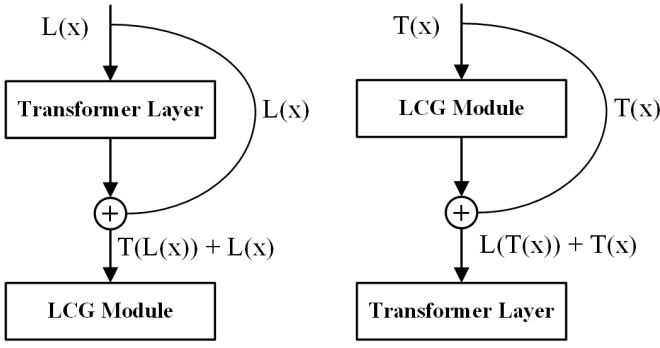


Fig. 3. The transformer layer and the LCG module interact each other.

Therefore, according to Eq. (2), the initial embedding sequence of i -th patch is constructed as follows:

$$X_i^{init} = [x_i^1 E, x_i^2 E, \dots, x_i^m E, \dots, x_i^n E] + E_{pos}. \quad (2)$$

For ease of description, the embedding sequence definition is assumed to be identical on each patch. Specifically, we define the node with d' dimensions features as $V = [v_1, v_2, \dots, v_m, \dots, v_n] \in \mathbb{R}^{n \times d'}$, where the m -th node $v_m = x^m E + E_{pos}^m \in \mathbb{R}^{d'}$ and $m \in [1, 2, \dots, n]$. Then, a spatial graph of every patch can be described as $G = \{V \in \mathbb{R}^{n \times d'}, E \in \mathbb{R}^{n \times n}\}$. The spatial graph's edges are constructed according to Eq. (3), as follows:

$$E_{v_i, j} = \frac{\exp(F_{\cos}(v_i, v_j))}{\sum_{k=1}^n \exp(F_{\cos}(v_i, v_k))}, \quad (3)$$

where $i, j \in [1, 2, \dots, n]$; $E_{v_i, j}$ is the edge between the node v_i and the node v_j in a patch. $F_{\cos}(v_i, v_j)$ means similarity score of the node v_i and the node v_j . Moreover, it has been empirically shown that the score of the cosine distance F_{\cos} is more effective in computing the correlation. And the cosine distance F_{\cos} is calculated according to Eq. (4), as follows:

$$F_{\cos}(v_i, v_j) = \frac{v_i \cdot v_j}{\|v_i\| \|v_j\|}, \quad (4)$$

where \cdot and $\|\cdot\|$ respectively denote element-wise multiplication operation and L2 regularization.

From Eq. (2), Eq. (3) and Eq. (4), we can easily obtain the graph's adjacency matrix $A_{i, j} = E_{v_i, j} \in \mathbb{R}^{n \times n}$ in a patch. To effectively mine and learn the relationship between discriminative local features, we adopt the graph network to aggregate and update nodes by information propagation from each node to its neighbors' nodes in the graph. And the aggregation node U of i -th graph is updated according to Eq. (5), as follows:

$$U = (D^{-\frac{1}{2}} A D^{-\frac{1}{2}} X_i) \cdot W, \quad (5)$$

where $A \in \mathbb{R}^{n \times n}$ is the adjacent matrix and $D \in \mathbb{R}^{n \times n}$ is the degree matrix of A ; The \cdot and $W \in \mathbb{R}^{n \times d'}$ represent an element-wise multiplication operation and a learnable parameter, respectively. It is worth noted that we use standard 2D learnable parameters W since we have not observed significant performance gains from using more advanced 3D learnable parameters W . In other words, $W \in \mathbb{R}^{n \times d'}$ is shared for

TABLE I
THE NODE CONFIGURATION FOR LCG MODULES.

	Sampling Size ($S \times S$)	Number (m)	Dimension (d)
Stage 1	2×2	64	12
Stage 2	4×4	16	48
Stage 3	8×8	4	192

N graphs of a patch, which significantly reduces parameter calculation complexity.

From Eq. (5), both a node itself and its neighbor nodes are aggregated and updated according to the learnable weight W to feed more local information. To introduce non-linearities and improve the convergence graph network, the node U is enhanced according to Eq. (5), as follows:

$$O = GELU(LN(U)), \quad (6)$$

where $GELU$ represents the gaussian error linear units (GELU) and LN denotes the layer normalization (LN); There is nothing special about choosing GELU and LN functions, just to be consistent with the original transformer layer's functions. According to the Eq. (6), $O \in \mathbb{R}^{n \times d'}$ replaces U as the new node with discriminative local features of a graph.

C. Transformer Layer

The transformer layer is used to model the global features between the different patches, consisting of a multi-head self-attention (MHSA) and a multi-layer perceptron (MLP) block. Assume that $X \in \mathbb{R}^{N \times M}$ is N patches, where $M = P^2 \times C$. The (P, P) is the size of each image patch and C is the number of channels. The $X \in \mathbb{R}^{N \times M}$ are linearly transformed to queries $Q \in \mathbb{R}^{N \times M_q}$, keys $K \in \mathbb{R}^{N \times M_k}$ and values $V \in \mathbb{R}^{N \times D_v}$. The scaled dot-product self-attention is applied on Q, K, V according to the Eq. (7), as follows:

$$\text{Attention}(Q, K, V) = \text{softmax}\left(\frac{QK^T}{\sqrt{M_v}}\right)V. \quad (7)$$

The MHSA splits the queries, keys, and values for h times and performs the h times self-attention function in parallel. Then the output values of each head are concatenated and linearly projected to form the final output. Therefore, according to Eq. (8) and Eq. (9), The output of transformer layer $Y \in \mathbb{R}^{N \times M}$ is calculated as follows:

$$X' = MSA(LN(X)) + X, \quad (8)$$

$$Y = MLP(LN(X')) + X'. \quad (9)$$

From Eq. (7), Eq. (8) and Eq. (9), one can see that since the transformer layer models global features on all patches, the proposed LCG module is essential for local feature learning.

D. Graph Interactive Transformer

As shown in Figure 2, the graph interactive transformer (GiT) method has l GiT blocks. Every GiT block consists of a local correlation graph (LCG) module and a transformer layer. It is worth noting that our proposed GiT block can make the global features of the transformer layer and the local

features of the LCG module form a coupling state. In other words, global features and local features can interact with each other in the entire feature learning process, as shown in Figure 3. Specifically, as describe in section III-B, assume that $O^l \in \mathbb{R}^{N \times n \times d'}$ represents the LCG module of the l -th GiT block has N graph with discriminatory local feature. And each graph is composed of n nodes with d' dimensional features. When embedding local features in the patch, we set $d' = d$. According to Eq. (10), the discriminative local feature O^l can be seamlessly converted into feature X^l of a patch.

$$X^l = \text{Reshape}(O^l) \quad (10)$$

where the $O^l \in \mathbb{R}^{N \times m \times d'}$ and the $X^l \in \mathbb{R}^{N \times D}$. From node to patch, the O^l can be reshape N patches with D dimensions features and $l \in [1, 2, \dots, 12]$ in this paper.

Let's forget about specific formulas of section III-B and section III-C, the l -th GiT blocks' LCG module $L(l)$ and transformer layer $T(l)$ are defined according to Eq. (11) and Eq. (12), as follows:

$$L^{(l)} = \text{LCG}(L^{(l-1)}, T^{(l-1)}), l \geq 2 \quad (11)$$

$$T^{(l)} = \text{Transformer}(T^{(l-1)}, L^{(l)}), l \geq 2 \quad (12)$$

From the Eq. (11) and Eq. (12), in the l -th GiT block, the LCG module learns local features from local and global features resulting from the LCG module and transformer layer of the $(l-1)$ -th GiT block. Similarly, the transformer layer learns global features from the global features generated by the transformer layer of the $(l-1)$ -th GiT block and the new local features outputted via the LCG module of the l -th GiT block. Therefore, GiT blocks' LCG modules and transformer layers are in a coupled status, bringing effective cooperation between local and global features.

Besides, the GiT method has three stages and every stage has 4 GiT blocks to handle feature maps of a specific scale. Each GiT block has the same architecture. It's just that the number of nodes n and the sampling size (S, S) are different in different stages. In the subsequent experiments, each image patch's resolution is the same as the ViT [28] method, i.e., the size of each patch is $(16, 16)$. The specific configuration of the node size in the LCG module is shown in Table I.

E. Loss Function Design

From Figure 2, the class token of the last GiT block serves as the image's vehicle feature representation. Inspired by BNNeck [51] in the CNN, we introduce it after the final class token. The features of the class token are directly applied to triplet loss of soft margin. After the feature of batch normalization (BN) is fed to cross-entropy loss without label smoothing. Therefore, the proposed GiT's total loss function is formulated as follows:

$$L_{total} = \alpha L_{CE} + \beta L_{Triplet}, \quad (13)$$

where L_{CE} and L_T respectively denote cross-entropy loss and triplet loss. α and β are manually setting constants used to keep balance of two loss functions. To avoid excessive tuning

those constants, we set $\alpha = \beta = 1$ in following experiments. The cross-entropy loss function [52] is formulated as follows:

$$L_{CE}(X, l) = \frac{-1}{M} \sum_{i=1}^M \sum_{j=1}^K (l_i, j) \log\left(\frac{e^{W_j^T X_i}}{\sum_{k=1}^K e^{W_k^T X_i}}\right), \quad (14)$$

where X is a training set and l is the class label information; M is number of training samples; K is the number of classes; (X_i, l_i) is the i -th training sample and $l_i \in \{1, 2, 3, \dots, K\}$; $W = [W_1, W_2, W_3, \dots, W_K]$ is a learn-able parameter matrix.

The triplet loss function [53] is formulated as follows:

$$L_{Triplet}(X^a, X^n, X^p) = \frac{-1}{M} \sum_{i=1}^M \max(\|X_i^a - X_i^n\|_2 - \|X_i^a - X_i^p\|_2, 0), \quad (15)$$

where (X^a, X^n, X^p) is a set of training triples; M is number of training triplets; for the i -th training triplet, (X_i^a, X_i^n) is a negative pair holding different class labels, and (X_i^a, X_i^p) is a positive pair having the same class label; $\|\cdot\|_2$ denotes the an Euclidean distance. Moreover, the hard sample mining [53] strategy is applied to improve the triplet loss, which aims to find the most difficult positive and negative image pairs in each mini-batch.

IV. EXPERIMENT AND ANALYSIS

To validate the proposed GiT method's superiority, it is compared with multiple state-of-the-art vehicle re-identification approaches on three large-scale datasets, namely, VeRi776 [32], VehicleID [33] and VeRi-Wild [34]. The rank-1 identification rate (R1) [32, 33, 54] and mean average precision (mAP) [12, 55–57] are used to assess the accuracy performance.

A. Datasets

VeRi776 [32] is captured by 20 cameras in unconstrained traffic scenarios, and each vehicle is captured by 2-18 cameras. Following the evaluation protocol of [32], VeRi776 is divided into a training subset containing 37,746 images of 576 subjects and a testing subset including a probe subset of 1,678 images of 200 subjects and a gallery subset of 11,579 images of the same 200 subjects. Moreover, only cross-camera vehicle pairs are evaluated. Suppose the same camera captures a probe image and a gallery image. In that case, the corresponding result will be excluded from the evaluation process.

VehicleID [33] includes 221,763 images of 26,267 subjects. Each vehicle is captured from either front or rear viewpoint. The training subset consists of 110,178 images of 13,164 subjects. There are three testing subsets, i.e., Test800, Test1600 and Test2400, for evaluating the performance at different data scales. Specifically, Test800 includes 800 gallery images and 6,532 probe images of 800 subjects. Test1600 contains 1,600 gallery images and 11,395 probe images of 1,600 subjects. Test2400 is composed of 2,400 gallery images and 17,638 probe images of 2,400 subjects. Moreover, for three testing subsets, the division of probe and gallery subsets is implemented as follows: randomly selecting one image of a subject to form the probe subset. All remaining images of this subject are used to construct the gallery subset. This division

TABLE II

THE PERFORMANCE (%) COMPARISON ON VERI776. THE RED, GREEN AND BLUE ROWS REPRESENT THE 1ST, 2ND AND 3RD PLACES, RESPECTIVELY.

Methods		R1	mAP
Proposed	GiT	96.86	80.34
Global + Local* (CNN & GN)	PCRNet [24]	95.40	78.60
	SGAT [26]	89.69	65.66
Global + Local (Pure CNN)	SAVER [58]	96.40	79.60
	VOC-ReID [59]	96.30	79.70
	PVEN [60]	95.60	79.50
	App+License [61]	95.41	78.08
	CFVMNet [62]	95.30	77.06
	SFF+SAtt [15]	94.93	74.11
	Part Regular [18]	94.30	74.30
	SAN [14]	93.30	72.50
	PAMTRI [23]	92.86	71.88
	MRM [63]	91.77	68.55
	DMML [64]	91.20	70.10
	VANet [39]	89.78	66.34
	AAVER [21]	88.97	61.18
	QD-DLF [12]	88.50	61.83
	VAMI [65]	85.92	61.32
Global (Pure CNN)	SDC-CNN [4]	83.49	53.45
	VST Path Proposals [5]	83.49	58.27
	PROVID [2]	81.56	53.42
	DenseNet121 [6]	80.27	45.06
	OIFE+ST [7]	68.30	51.42
	FACT [1]	52.21	18.75
	GoogLeNet [66]	52.32	17.89
VGG-CNN-M-1024 [33]	44.10	12.76	

is repeated and evaluated 10 times, and the average result is reported as the final performance.

VeRi-Wild [34] is newly dataset released in CVPR 2019. Different to the VeRi776 [32] and VehicleID [33] captured at day, its images captured at both day and night. VeRi-Wild contains 416,314 images of 40,671 subjects in total. It is divided into a training subset of 277,797 images of 30,671, and a testing subset of 128,517 images of 10,000 subjects. Similar to VehicleID [33], the testing subset is organized into three different scale subsets, i.e., Test3000, Test5000, and Test10000. To be more specific, Test3000 is composed of 41,816 gallery images and 3000 probe images of 3,000 subjects. Test5000 is made up of 69,389 gallery images and 5,000 probe images of 5,000 subjects. Test10000 is consisted of 138,517 gallery images and 10,000 probe images of 10,000 subjects.

B. Implementation Details

The deep learning toolbox is PyTorch [67] with FP16 training. Training configurations are summarized as follows. (1) We respectively use ImageNet pre-trained weights of ViT and a truncated normal distribution initialize to the transformer layers and the LCG modules. (2) Random erasing [68] and z-score normalization are used for the data augmentation. Both probabilities of horizontal flip and random erasing are set to 0.5. (3) The mini-batch stochastic gradient descent (SGD) method [69] is applied to train parameters. The weight decays are set to 1×10^{-4} and the momentums are set to 0.9. There are 150 epochs for the training process. The learning rates are initialized to 1×10^{-4} , and they are linearly warmed up [51] to 1×10^{-2} in the first 5 epochs. After warming up, the

TABLE III

THE PERFORMANCE (%) COMPARISON ON VEHICLEID. THE RED, GREEN AND BLUE ROWS REPRESENT THE 1ST, 2ND AND 3RD PLACES, RESPECTIVELY.

Methods		Test800		Test1600		Test2400		
		R1	mAP	R1	mAP	R1	mAP	
Proposed	GiT	84.65	90.12	80.52	86.77	77.94	84.26	
Global + Local* (CNN & GN)	HPGN [27]	83.91	89.60	79.97	86.16	77.32	83.60	
	SGAT [26]	78.12	81.49	73.98	77.46	71.87	75.35	
	HSS-GCN [25]	72.70	77.30	67.90	72.40	62.40	66.10	
Global + Local (Pure CNN)	CFVMNet [62]	81.40	N/A	77.30	N/A	74.70	N/A	
	App+License [61]	79.50	82.70	76.90	79.90	74.80	77.70	
	SAVER [58]	79.90	N/A	77.60	N/A	75.30	N/A	
	MGL [70]	79.60	82.10	76.20	79.60	73.00	75.50	
	Part Regular [18]	78.40	N/A	75.00	N/A	74.20	N/A	
	PRN[11]	78.92	N/A	74.94	N/A	71.58	N/A	
	MSV [43]	75.10	79.30	71.80	75.40	68.70	73.30	
	DQAL [71]	74.74	N/A	71.01	N/A	68.23	N/A	
	EALN [44]	75.11	77.50	71.78	74.20	69.30	71.00	
	AAVER [21]	74.69	N/A	68.62	N/A	63.54	N/A	
	QD-DLF [12]	72.32	76.54	70.66	74.63	64.14	68.41	
	TAMR [17]	66.02	N/A	62.90	N/A	59.69	N/A	
	VAMI [65]	63.12	N/A	52.87	N/A	47.34	N/A	
	Global (Pure CNN)	SDC-CNN [4]	56.98	63.52	50.57	57.07	42.92	49.68
		MAD+STR [38]	N/A	82.20	N/A	75.90	N/A	72.80
PMSM [20]		N/A	64.20	N/A	57.20	N/A	51.80	
DJDL [37]		72.30	N/A	70.80	N/A	68.00	N/A	
DenseNet121 [6]		66.10	68.85	67.39	69.45	63.07	65.37	
OIFE+ST [7]		N/A	N/A	N/A	N/A	67.00	N/A	
DRDL [33]		48.91	N/A	46.36	N/A	40.97	N/A	
FACT [1]	49.53	N/A	44.63	N/A	39.91	N/A		

learning rates are maintained at 1×10^{-2} from 11th to 50th epochs. Then, the learning rates are reduced to 1×10^{-3} from 51st to 85th epochs, it decays to 1×10^{-4} after 85 epochs and further dropped to 1×10^{-5} between 120th and 150th epochs. (4) Unless otherwise specified, each mini-batch includes 8 subjects and each subject holds 6 images.

During the testing phase, those 768-dimensional features resulted from the BN layer (see Figure 2) as the vehicle images' final features. Moreover, the Cosine distance of those the final features is applied as the similarity measurement for vehicle re-identification.

C. Comparison with State-of-the-art Methods

According to the development process of vehicle re-identification, those state-of-the-art methods under comparison are roughly classified into three categories for a clear presentation. Specifically, Global denotes the approaches [1, 2, 4–7, 20, 33, 37, 38, 66] exploiting global features based on pure convolutional neural network (CNN); Global + Local represents the methods [12, 14, 15, 18, 21, 23, 39, 58–65] utilizing global features and local features based on pure CNN; Global + Local* denotes the approaches [24, 26, 27] dealing with global features and local features based on CNN and graph network (GN).

1) *Comparisons on VeRi776*: Table II shows the performance comparison of the proposed GiT method and multiple state-of-the-art approaches on VeRi776 dataset. It can be found that the proposed GiT method achieves the highest rank-1 (R1) identification rate (i.e., 96.86%) and mAP (i.e., 80.34%). As shown in Table II, the method of combining global and local features (i.e., Global + Local and Global + Local*) are mostly

TABLE IV

THE PERFORMANCE (%) COMPARISON ON THE VERI-WILD. THE RED, GREEN AND BLUE ROWS REPRESENT THE 1ST, 2ND AND 3RD PLACES, RESPECTIVELY.

Methods		Test3000		Test5000		Test10000	
		R1	mAP	R1	mAP	R1	mAP
Proposed	GiT	92.65	81.76	89.92	75.64	85.41	67.55
Global + Local* (CNN & GN)	PCRNet [24]	92.50	81.20	89.60	75.30	85.00	67.10
	HPGN [27]	91.37	80.42	88.21	75.17	82.68	65.04
Global + Local (Pure CNN)	GLAMOR [72]	92.10	77.15	N/A	N/A	N/A	N/A
	UMTS [73]	84.50	72.70	79.30	66.10	72.80	54.20
	DFLNet [74]	80.68	68.21	70.67	60.07	61.60	49.02
	AAVER [21]	75.80	62.23	68.24	53.66	58.69	41.68
Global (Pure CNN)	FDA-Net [34]	64.03	35.11	57.82	29.80	49.43	22.78
	GSTE [75]	60.46	31.42	52.12	26.18	45.36	19.50
	GoogLeNet [9]	57.16	24.27	53.16	24.15	44.61	21.53
	HDC [76]	57.10	29.14	49.64	24.76	43.97	18.30
	DRDL [33]	56.96	22.50	51.92	19.28	44.60	14.81
	Softmax [32]	53.40	26.41	46.16	22.66	37.94	17.62
	Triplet [77]	44.67	15.69	40.34	13.34	33.46	9.93

superior to the method of only using global features (Global) on the VeRi776 dataset by a large margin. For example, the best Global + Local* method (i.e., PCRNet [24]) and the best Global + Local method (i.e., SAVER [58]) respectively defeats the best Global method (i.e., SDC-CNN [4]) by 11.91 % and 12.91% in term of R1 identification rate. This demonstrates that part details and local features are important clues for vehicle re-identification. Meanwhile, the R1 identification rate and mAP of the GiT approach exceeds 13.37% and 26.89 % over the best Global method (i.e., SDC-CNN [4]).

Moreover, among those compared state-of-the-art methods, the proposed GiT approach outperforms the best Global + Local* method (i.e., PCRNet [24]) and the best Global + Local method. For example, the proposed GiT method respectively higher 1.46% and 1.74% than the best Global + Local* method (i.e., PCRNet [24]) on R1 identification rate and mAP. It is noted that the PCRNet [24] extra uses an image segmentation model trained on vehicle parsing data as a preprocessing tool to obtain the parsed masks of vehicle images, while GiT does not use any extra semantic annotation information.

2) *Comparisons on VehicleID*: Table III shows the rank-1 identification rate (R1) and mAP comparison of the proposed GiT method and state-of-the-art approaches on the VehicleID [33] dataset with a more significant number of images than the VeRi776 [32] dataset. Three different type of testing subsets are evaluated, including Test800, Test1600, and Test2400. It can be found that the proposed GiT method consistently outperforms those state-of-the-art methods under comparison. More analysis are described as follows.

First, on this large scale dataset, the Global methods [1, 4, 6, 7, 20, 33, 37, 38] can not acquire promising accuracies, which are inferior to the proposed GiT method and other methods used local features. Second, the proposed GiT method has better performance than those Global + Local methods. For example, taking the best Global + Local method, i.e., App+License [61], it is still defeated by the GiT method, as it has lower rank-1 identification rates and mAP on three different testing subsets (i.e., Test800, Test1600 and Test2400). Third, the proposed GiT method is superior to Global + Local*

TABLE V

THE ABLATION STUDY OF OUR GiT METHOD ON THE VERI776 AND VEHICLEID DATASETS.

Names	VeRi776		VehicleID					
	R1	mAP	Test800	Test1600	Test2400			
	R1	mAP	R1	mAP	R1	mAP		
Baseline (Global)	95.84	78.92	82.41	87.05	76.36	83.29	73.31	80.10
GiT (No Interactive)	96.17	79.55	83.26	88.88	79.05	85.29	76.22	82.50
GiT (Global → Local)	96.34	79.78	83.57	89.13	79.29	85.52	76.46	82.61
GiT (Global ← Local)	96.42	79.87	83.61	89.16	79.43	85.66	76.75	82.97
GiT (Interactive)	96.86	80.34	84.65	90.12	80.52	86.77	77.94	84.26

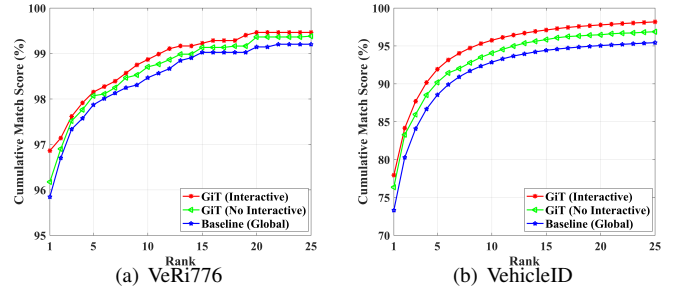


Fig. 4. The CMC curves on VeRi776 and VehicleID datasets

methods. For example, on the largest Test2400 subset, the proposed GiT's R1 identification rate and mAP are respectively higher 0.62% and 0.78% than that of the best Global + Local* methods, i.e., HPGN [27].

3) *Comparisons on VeRi-Wild*: Table IV shows the comparison result on VeRi-Wild [34] dataset. Among those methods, it can be found that the proposed GiT method obtains the 1st place again on the Test3000, Test5000, and Test1000 of VeRi-Wild dataset. For example, on largest Test1000 subset, R1 and mAP of GiT method respectively are 0.41% and 0.45% higher than those of the 2nd place method, i.e., PCRNet [24], which extra uses an image segmentation model. Compared with the 3rd place method (i.e., HPGN [27]), the proposed GiT method defeats it by 2.73% in term of mAP and 2.51% in term of R1 identification rate on largest Test1000 subset. Meanwhile, the proposed GiT method obtains the state-of-the-art performance on VeRi776, VehicleID, and VeRi-Wild, which shows the effectiveness and generalization of our method. Besides, one can see that a lot of approaches (the Global + Local [21, 72–74] and the Global + Local*[24, 27]) have made significant progress than the Global method [9, 32–34, 75–77] on the VeRi-Wild dataset. Those results also reflect the trend that the methods which exploit both global and local features achieve better results than early Global methods that only use global features.

D. Ablation Studies and Analysis

The comparison results presented in Tables II, III, and IV demonstrate that the proposed GiT method is superior to many state-of-the-art vehicle re-identification methods. Recall Figure 2, the proposed GiT method is mainly made up of pure transformer layers for learning global features and local correlation graph (LCG) modules for mining local features. Moreover, the LCG module's local features and global features

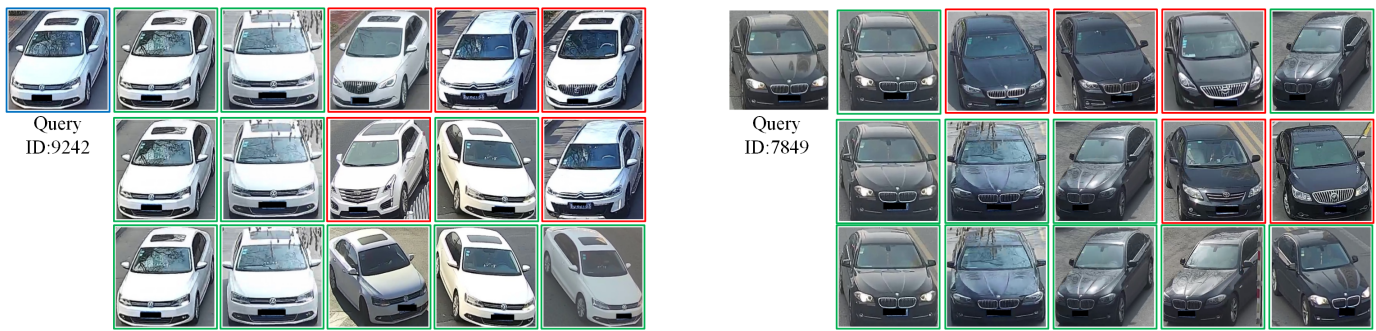


Fig. 5. Rank-5 visualization examples on VeRi-Wild. The first, second, and third rows show the top five images returned by Baseline (Global), GiT (No Interactive), and GiT (Interactive), respectively.

TABLE VI
THE PERFORMANCE (%) COMPARISON AMONG DIFFERENT SAMPLING SIZES FOR FEATURE MAP IN THE GiT METHOD.

Names	Sampling Sizes	VeRi776		Test800		VehicleID				Test3000		VeRi-Wild		Test10000	
		R1	mAP	R1	mAP	R1	mAP	R1	mAP	R1	mAP	R1	mAP	R1	mAP
GiT1	(2, 2)→(2,2)→(2,2)	96.51	79.88	84.01	89.25	79.44	85.93	76.82	83.17	91.54	80.79	88.80	74.56	84.12	66.31
GiT2	(4, 4)→(4,4)→(4,4)	96.44	79.71	83.69	89.13	79.30	85.64	76.61	82.83	91.35	80.42	88.67	74.17	83.85	66.08
GiT3	(8, 8)→(8,8)→(8,8)	96.33	79.62	83.38	88.91	79.17	85.35	76.36	82.61	91.19	80.03	88.28	73.64	83.19	65.26
GiT	(2,2)→(4,4)→(8,8)	96.86	80.34	84.65	90.12	80.52	86.77	77.94	84.26	92.65	81.76	89.92	75.64	85.41	67.55

of the transformer layer can interact and improve each other. In what follows, the proposed GiT method is comprehensively analyzed from two aspects to investigate the logic behind its superiority. (1)The role of LCG module and transformer layer interaction. (2) The influence of changing feature map’s sampling size in LCG module.

1) The Role of LCG Module and Transformer Layer Interaction.: We conduct the ablation study of the components in the GiT on the vehicle dataset. Baseline (Global) denotes the method that uses pure transformer layers without local correlation graph (LCG) modules. GiT (No Interactive) represents the method applies GiT without the red and blue lines of all GiT blocks in Figure 2. And similar to Figure 1 (c), global features and local features are separately supervised with two loss functions. GiT (Global → Local) means the method utilizes GiT without the red lines of all GiT blocks in Figure 2. GiT (Global ← Local) denotes the method employs GiT without the blue lines of all GiT blocks in Figure 2. GiT (Interactive) indicates the full version of GiT, i.e., the red line and blue line are used simultaneously.

Firstly, as can be seen in Table V, the GiT (No Interactive), GiT (Global → Local), GiT (Global ← Local) and GiT have all consistently outperformed Baseline (Global) on two datasets. This means that we proposed LCG modules that can learn discriminative local features. The global appearances and local details are complementary for discriminative representations. Secondly, the result of GiT (Global → Local) and GiT (Global ← Local) are better than GiT (No Interactive) by more than 0.23% and 0.32% mAP on the VeRi776 dataset, respectively. Furthermore, the proposed GiT (Interactive) outperforms both GiT (Global → Local) and GiT (Global ← Local) on two datasets. For example, compared to the GiT (Global → Local) and GiT (Global ← Local),

on VeRi776, the GiT (Interactive) holds a larger 0.52% and 0.44% R1 identification rate, respectively. And on Test2400 of VehicleID, the GiT holds a larger 1.65% and 1.29 % mAP, respectively. Thirdly, from Figure 4, it can be intuitively found that from rank-1 to rank-25, the proposed GiT (Interactive) is better than Baseline (Global) and GiT (No Interactive) on VeRi776 [32] and Test2400 of VehicleID [33] datasets by a large margin. These results demonstrate that the interaction of that transformer layer and LCG module can effectively improve the performance of vehicle re-identification.

In particular, to visualize our proposed GiT (Interactive) method’s effectiveness, the rank-5 retrieval results of two example query images from VeRi-Wild are shown in Figure 5. The first, second, and third rows respectively show the top five images returned by Baseline (Global), GiT (No Interactive), and GiT (Interactive). Images with blue boxes denote queries. The images with green boxes and red boxes are correct and incorrect retrieve results, respectively. It can be seen that the GiT (Interactive) performed well and retrieved the vehicle images with discriminative parts from the query images accurately. The GiT (No Interactive) method ranks second, while the baseline method has poor results. This shows that the necessity and effectiveness of global appearances and local information interaction for vehicle re-identification.

2) The Influence of Changing Feature Map’s Sampling Size in LCG Module.: In the LCG module, the proposed GiT method divides an image into 16×16 sized patches and the sampling size determines the node how to establish local correlation. So we also compare the performance between the designed LCG module with a different sampling size of feature map (e.g., 2, 4, and 8) on the proposed GiT method as shown in Table VI. Three GiTs of the different sampling sizes of feature map configured LCG module. Specifically,

in Table VI, the GiT denotes that the progressive sampling size setting is $(2, 2) \rightarrow (4, 4) \rightarrow (8, 8)$, which means that with the depth increases, every 4 GiT blocks is a stage. Each stage uses the same sampling size, which is $(2, 2)$, $(4, 4)$ and $(8, 8)$ respectively. Moreover, The GiT1 represents that when sampling size setting is $(2, 2)$, which means that the sampling size is fixed to be 2×2 and does not change among with the depth. Both $(4, 4)$ and $(8, 8)$ sampling size settings hold the same rule of the $(2, 2)$ sampling size setting, respectively, namely GiT2 and GiT3.

From Table VI, the GiT of progressive sampling size is always better performance than the fixed sampling size on three different datasets. For example, on the largest Test 10000 of VeRi-Wild, GiT's mAP is 1.24%, 1.47% and 2.29% higher than that of GiT1, GiT2 and GiT3, respectively. On the largest Test2400 of VehicleID, GiT defeats GiT1, GiT2 and GiT3 by 1.12%, 1.33% and 1.58% higher R1 identification rates, respectively. These results prove that appropriately changing the sampling size can help promote vehicle re-identification performance. Besides, comparing GiT1, GiT2 and GiT3, it can be interestingly found that the three methods' performance is consistent (i.e., $\text{GiT1} > \text{GiT2} > \text{GiT3}$) on VeRi776, VehicleID, and VeRi-Wild datasets. For example, on the largest Test 10000 of VeRi-Wild, the GiT1 method of fixed sampling size $(2, 2)$ respectively higher 0.93% and 1.05% than the GiT3 method of fixed sampling size 16×16 on R1 identification rate and mAP. These results demonstrate that if the fixed sampling size is used, the $(2, 2)$ sampling size is more competitive.

V. CONCLUSION

In this paper, we propose a graph interactive transformer (GiT) method for vehicle re-identification. The GiT method couples graphs and transformers to explore the interaction between local features and global features, resulting in effective cooperation between local and global features. We also design a new local correlation graph (LCG) module for learning local features within patches. We construct extensive experiments to analyze our GiT method, including: (1) comparing to a lot of state-of-the-art approaches to demonstrate the GiT method's superiority; (2) the ablation study of the positive role of exploring the interaction between local features and global features; (3) the influence of local correlation graph using different sampling configurations. Besides, the proposed GiT method is the first work to combine graphs and transformers for vehicle re-identification to the best of our knowledge.

REFERENCES

- [1] X. Liu, W. Liu, H. Ma, and H. Fu, "Large-scale vehicle re-identification in urban surveillance videos," in *International Conference on Multimedia & Expo*, 2016, pp. 1–6.
- [2] X. Liu, W. Liu, T. Mei, and H. Ma, "Provid: Progressive and multi-modal vehicle re-identification for large-scale urban surveillance," *IEEE Transactions on Multimedia*, vol. 20, no. 3, pp. 645–658, 2018.
- [3] X. Liu, S. Zhang, Q. Huang, and W. Gao, "Ram: a region-aware deep model for vehicle re-identification," in *International Conference on Multimedia & Expo*, 2018, pp. 1–6.
- [4] J. Zhu, H. Zeng, Z. Lei, L. Zheng, and C. Cai, "A shortly and densely connected convolutional neural network for vehicle re-identification," in *International Conference on Pattern Recognition*, 2018, pp. 3285–3290.
- [5] Y. Shen, T. Xiao, H. Li, S. Yi, and X. Wang, "Learning deep neural networks for vehicle re-id with visual-spatio-temporal path proposals," in *International Conference on Computer Vision*, 2017, pp. 1918–1927.
- [6] G. Huang, Z. Liu, L. van der Maaten, and K. Q. Weinberger, "Densely connected convolutional networks," in *Conference on Computer Vision and Pattern Recognition*, 2017, pp. 2261–2269.
- [7] Z. Wang, L. Tang, X. Liu, Z. Yao, S. Yi, J. Shao, J. Yan, S. Wang, H. Li, and X. Wang, "Orientation invariant feature embedding and spatial temporal regularization for vehicle re-identification," in *International Conference on Computer Vision*, 2017, pp. 379–387.
- [8] K. Simonyan and A. Zisserman, "Very deep convolutional networks for large-scale image recognition," in *International Conference on Learning Representations*, 2015.
- [9] C. Szegedy, W. Liu, Y. Jia, P. Sermanet, S. Reed, D. Anguelov, D. Erhan, V. Vanhoucke, and A. Rabinovich, "Going deeper with convolutions," in *Conference on Computer Vision and Pattern Recognition*, 2015, pp. 1–9.
- [10] K. He, X. Zhang, S. Ren, and J. Sun, "Identity mappings in deep residual networks," *European Conference on Computer Vision*, pp. 630–645, 2016.
- [11] H. Chen, B. Lagadec, and F. Bremond, "Partition and reunion: A two-branch neural network for vehicle re-identification," in *Conference on Computer Vision and Pattern Recognition Workshops*, 2019, pp. 184–192.
- [12] J. Zhu, H. Zeng, J. Huang, S. Liao, L. Zhen, C. Cai, and L. Zheng, "Vehicle re-identification using quadruple directional deep learning features," *Transactions on Intelligent Transportation Systems*, vol. 21, no. 1, pp. 410–420, 2020.
- [13] J. Zhu, J. Huang, H. Zeng, X. Ye, B. Li, Z. Lei, and L. Zheng, "Object re-identification via joint quadruple decorrelation directional deep networks in smart transportation," *IEEE Internet of Things Journal (Early Access)*, 2019.
- [14] J. Qian, W. Jiang, H. Luo, and H. Yu, "Stripe-based and attribute-aware network: A two-branch deep model for vehicle re-identification," *arXiv preprint arXiv:1910.05549*, 2019.
- [15] C. Liu, D. Q. Huynh, and M. Reynolds, "Urban area vehicle re-identification with self-attention stair feature fusion and temporal bayesian re-ranking," in *International Joint Conference on Neural Networks*, 2019, pp. 1–8.
- [16] X. Ma, K. Zhu, H. Guo, J. Wang, M. Huang, and Q. Miao, "Vehicle re-identification with refined part model," in *International Conference on Multimedia & Expo Workshops*, 2019, pp. 603–606.
- [17] H. Guo, K. Zhu, M. Tang, and J. Wang, "Two-level attention network with multi-grain ranking loss for vehicle re-identification," *IEEE Transactions on Image Processing*, pp. 4328–4338, 2019.
- [18] B. He, J. Li, Y. Zhao, and Y. Tian, "Part-regularized near-duplicate vehicle re-identification," in *Conference on Computer Vision and Pattern Recognition*, 2019, pp. 3997–4005.
- [19] X. Zhang, R. Zhang, J. Cao, D. Gong, M. You, and C. Shen, "Part-guided attention learning for vehicle re-identification," *arXiv preprint arXiv:1909.06023*, 2019.
- [20] Y. Sun, M. Li, and J. Lu, "Part-based multi-stream model for vehicle searching," in *International Conference on Pattern Recognition*, 2018, pp. 1372–1377.
- [21] P. Khorramshahi, A. Kumar, N. Peri, S. S. Rambhatla, J.-C. Chen, and R. Chellappa, "A dual-path model with adaptive attention for vehicle re-identification," in *International Conference on Computer Vision*, 2019, pp. 6132–6141.
- [22] P. Khorramshahi, N. Peri, A. Kumar, A. Shah, and R. Chellappa, "Attention driven vehicle re-identification and unsupervised

- anomaly detection for traffic understanding,” in *Computer Vision and Pattern Recognition Workshops*, 2019, pp. 239–246.
- [23] Z. Tang, M. Naphade, S. Birchfield, J. Tremblay, W. Hodge, R. Kumar, S. Wang, and X. Yang, “Pamtri: Pose-aware multi-task learning for vehicle re-identification using highly randomized synthetic data,” in *International Conference on Computer Vision*, 2019, pp. 211–220.
- [24] X. Liu, W. Liu, J. Zheng, C. Yan, and T. Mei, “Beyond the parts: Learning multi-view cross-part correlation for vehicle re-identification,” in *Proceedings of the 28th ACM International Conference on Multimedia*, 2020, pp. 907–915.
- [25] Z. Xu, L. Wei, C. Lang, S. Feng, T. Wang, and A. G. Bors, “Hss-gcn: A hierarchical spatial structural graph convolutional network for vehicle re-identification,” in *Proc. ICPR’s Int. Workshop on Human and Vehicle Analysis for Intelligent Urban Computing (IUC)*. Springer, 2021.
- [26] Y. Zhu, Z.-J. Zha, T. Zhang, J. Liu, and J. Luo, “A structured graph attention network for vehicle re-identification,” in *Proceedings of the 28th ACM international conference on Multimedia*, 2020, pp. 646–654.
- [27] F. Shen, J. Zhu, X. Zhu, Y. Xie, and J. Huang, “Exploring spatial significance via hybrid pyramidal graph network for vehicle re-identification,” *IEEE Transactions on Intelligent Transportation Systems*, 2021.
- [28] A. Dosovitskiy, L. Beyer, A. Kolesnikov, D. Weissenborn, X. Zhai, T. Unterthiner, M. Dehghani, M. Minderer, G. Heigold, S. Gelly *et al.*, “An image is worth 16x16 words: Transformers for image recognition at scale,” *arXiv preprint arXiv:2010.11929*, 2020.
- [29] S. He, H. Luo, P. Wang, F. Wang, H. Li, and W. Jiang, “Transreid: Transformer-based object re-identification,” *arXiv preprint arXiv:2102.04378*, 2021.
- [30] X. Zhu, W. Su, L. Lu, B. Li, X. Wang, and J. Dai, “Deformable detr: Deformable transformers for end-to-end object detection,” *arXiv preprint arXiv:2010.04159*, 2020.
- [31] J. Chen, Y. Lu, Q. Yu, X. Luo, E. Adeli, Y. Wang, L. Lu, A. L. Yuille, and Y. Zhou, “Transunet: Transformers make strong encoders for medical image segmentation,” *arXiv preprint arXiv:2102.04306*, 2021.
- [32] X. Liu, W. Liu, T. Mei, and H. Ma, “A deep learning-based approach to progressive vehicle re-identification for urban surveillance,” in *European Conference on Computer Vision*, 2016, pp. 869–884.
- [33] H. Liu, Y. Tian, Y. Wang, L. Pang, and T. Huang, “Deep relative distance learning: Tell the difference between similar vehicles,” in *Conference on Computer Vision and Pattern Recognition*, 2016, pp. 2167–2175.
- [34] Y. Lou, Y. Bai, J. Liu, S. Wang, and L. Duan, “Veri-wild: A large dataset and a new method for vehicle re-identification in the wild,” in *Conference on Computer Vision and Pattern Recognition*, 2019, pp. 3235–3243.
- [35] K. Yan, Y. Tian, Y. Wang, W. Zeng, and T. Huang, “Exploiting multi-grain ranking constraints for precisely searching visually-similar vehicles,” in *International Conference on Computer Vision*, 2017, pp. 562–570.
- [36] Y. Zhang, D. Liu, and Z.-J. Zha, “Improving triplet-wise training of convolutional neural network for vehicle re-identification,” in *International Conference on Multimedia & Expo*, 2017, pp. 1386–1391.
- [37] Y. Li, Y. Li, H. Yan, and J. Liu, “Deep joint discriminative learning for vehicle re-identification and retrieval,” in *International Conference on Image Processing*, 2017, pp. 395–399.
- [38] N. Jiang, Y. Xu, Z. Zhou, and W. Wu, “Multi-attribute driven vehicle re-identification with spatial-temporal re-ranking,” in *International Conference on Image Processing*, 2018, pp. 858–862.
- [39] R. Chu, Y. Sun, Y. Li, Z. Liu, C. Zhang, and Y. Wei, “Vehicle re-identification with viewpoint-aware metric learning,” in *International Conference on Computer Vision*, 2019, pp. 8282–8291.
- [40] H. Guo, C. Zhao, Z. Liu, J. Wang, and H. Lu, “Learning coarse-to-fine structured feature embedding for vehicle re-identification,” in *AAAI Conference on Artificial Intelligence*, 2018, pp. 6853–6860.
- [41] R. Kumar, E. Weill, F. Aghdasi, and P. Sriram, “Vehicle re-identification: an efficient baseline using triplet embedding,” in *International Joint Conference on Neural Networks*, 2019, pp. 1–9.
- [42] A. Kanacı, X. Zhu, and S. Gong, “Vehicle re-identification in context,” in *German Conference on Pattern Recognition*, 2018, pp. 377–390.
- [43] Y. Xu, N. Jiang, L. Zhang, Z. Zhou, and W. Wu, “Multi-scale vehicle re-identification using self-adapting label smoothing regularization,” in *IEEE International Conference on Acoustics, Speech and Signal Processing*, 2019, pp. 2117–2121.
- [44] Y. Lou, Y. Bai, J. Liu, S. Wang, and L.-Y. Duan, “Embedding adversarial learning for vehicle re-identification,” *IEEE Transactions on Image Processing*, pp. 3794–3807, 2019.
- [45] J. Peng, H. Wang, F. Xu, and X. Fu, “Cross domain knowledge learning with dual-branch adversarial network for vehicle re-identification,” *Neurocomputing*, 2020.
- [46] Z. Zheng, T. Ruan, Y. Wei, Y. Yang, and T. Mei, “Vehiclenet: learning robust visual representation for vehicle re-identification,” *IEEE Transactions on Multimedia*, 2020.
- [47] J. Redmon, S. Divvala, R. Girshick, and A. Farhadi, “You only look once: Unified, real-time object detection,” in *Conference on Computer Vision and Pattern Recognition*, 2016, pp. 779–788.
- [48] A. M. N. Taufique and A. Savakis, “Labnet: Local graph aggregation network with class balanced loss for vehicle re-identification,” *arXiv preprint arXiv:2011.14417*, 2020.
- [49] D. Ji, H. Wang, H. Hu, W. Gan, W. Wu, and J. Yan, “Context-aware graph convolution network for target re-identification,” *arXiv preprint arXiv:2012.04298*, 2020.
- [50] C. Wang, H. Fu, and H. Ma, “Global structure graph guided fine-grained vehicle recognition,” in *ICASSP 2020 - 2020 IEEE International Conference on Acoustics, Speech and Signal Processing (ICASSP)*, 2020, pp. 1913–1917.
- [51] H. Luo, W. Jiang, Y. Gu, F. Liu, X. Liao, S. Lai, and J. Gu, “A strong baseline and batch normalization neck for deep person re-identification,” *IEEE Transactions on Multimedia (Early Access)*, 2019.
- [52] Z. Zheng, L. Zheng, and Y. Yang, “Unlabeled samples generated by gan improve the person re-identification baseline in vitro,” in *International Conference on Computer Vision*, 2017, pp. 3754–3762.
- [53] A. Hermans, L. Beyer, and B. Leibe, “In defense of the triplet loss for person re-identification,” *arXiv preprint arXiv:1703.07737*, 2017.
- [54] F. Shen, L. Lin, M. Wei, J. Liu, J. Zhu, H. Zeng, C. Cai, and L. Zheng, “A large benchmark for fabric image retrieval,” in *2019 IEEE 4th International Conference on Image, Vision and Computing*. IEEE, 2019, pp. 247–251.
- [55] L. Zheng, L. Shen, L. Tian, S. Wang, J. Wang, and Q. Tian, “Scalable person re-identification: A benchmark,” in *International Conference on Computer Vision*, 2015, pp. 1116–1124.
- [56] J. Zhu, H. Zeng, J. Huang, X. Zhu, Z. Lei, C. Cai, and L. Zheng, “Body symmetry and part locality guided direct nonparametric deep feature enhancement for person re-identification,” *IEEE Internet of Things Journal*, vol. 7, no. 3, pp. 2053–2065, 2020.
- [57] F. Shen, M. Wei, J. Liu, H. Zeng, and J. Zhu, “Rgb and lbp-texture deep nonlinearly fusion features for fabric retrieval,” *High Technology Letters*, vol. 26, no. 2, pp. 196–203, 2020.
- [58] P. Khorramshahi, N. Peri, J.-c. Chen, and R. Chellappa, “The devil is in the details: Self-supervised attention for vehicle re-identification,” in *European Conference on Computer Vision*. Springer, 2020, pp. 369–386.
- [59] X. Zhu, Z. Luo, P. Fu, and X. Ji, “Voc-reid: Vehicle re-

- identification based on vehicle-orientation-camera,” in *Proceedings of the IEEE Conference on Computer Vision and Pattern Recognition Workshops*, 2020, pp. 602–603.
- [60] D. Meng, L. Li, X. Liu, Y. Li, S. Yang, Z.-J. Zha, X. Gao, S. Wang, and Q. Huang, “Parsing-based view-aware embedding network for vehicle re-identification,” in *Proceedings of the IEEE Conference on Computer Vision and Pattern Recognition*, 2020, pp. 7103–7112.
- [61] Y. He, C. Dong, and Y. Wei, “Combination of appearance and license plate features for vehicle re-identification,” in *International Conference on Image Processing*, 2019, pp. 3108–3112.
- [62] Z. Sun, X. Nie, X. Xi, and Y. Yin, “Cfvmnet: A multi-branch network for vehicle re-identification based on common field of view,” in *Proceedings of the 28th ACM International Conference on Multimedia*, 2020, pp. 3523–3531.
- [63] J. Peng, H. Wang, T. Zhao, and X. Fu, “Learning multi-region features for vehicle re-identification with context-based ranking method,” *Neurocomputing*, vol. 359, pp. 427–437, 2019.
- [64] G. Chen, T. Zhang, J. Lu, and J. Zhou, “Deep meta metric learning,” in *International Conference on Computer Vision*, 2019, pp. 9547–9556.
- [65] Y. Zhou, L. Shao, and A. Dhabi, “Viewpoint-aware attentive multi-view inference for vehicle re-identification,” in *Conference on Computer Vision and Pattern Recognition*, 2018, pp. 6489–6498.
- [66] L. Yang, P. Luo, C. L. Chen, and X. Tang, “A large-scale car dataset for fine-grained categorization and verification,” in *Conference on Computer Vision and Pattern Recognition*, 2015, pp. 3973–3981.
- [67] A. Paszke, S. Gross, F. Massa, A. Lerer, J. Bradbury, G. Chanan, T. Killeen, Z. Lin, N. Gimelshein, L. Antiga, A. Desmaison, A. Kopf, E. Yang, Z. DeVito, M. Raison, A. Tejani, S. Chilamkurthy, B. Steiner, L. Fang, J. Bai, and S. Chintala, “Pytorch: An imperative style, high-performance deep learning library,” in *Advances in Neural Information Processing Systems*, 2019, pp. 8024–8035.
- [68] Z. Zhong, L. Zheng, G. Kang, S. Li, and Y. Yang, “Random erasing data augmentation,” *arXiv preprint arXiv:1708.04896*, 2017.
- [69] A. Krizhevsky, I. Sutskever, and G. E. Hinton, “Imagenet classification with deep convolutional neural networks,” in *Annual Conference on Neural Information Processing Systems*, 2012, pp. 1097–1105.
- [70] X. Yang, C. Lang, P. Peng, and J. Xing, “Vehicle re-identification by multi-grain learning,” in *International Conference on Image Processing*, 2019, pp. 3113–3117.
- [71] J. Hou, H. Zeng, J. Zhu, J. Hou, J. Chen, and K.-K. Ma, “Deep quadruplet appearance learning for vehicle re-identification,” *IEEE Transactions on Vehicular Technology*, vol. 68, no. 9, pp. 8512–8522, 2019.
- [72] A. Suprem and C. Pu, “Looking glamorous: Vehicle re-id in heterogeneous cameras networks with global and local attention,” *arXiv preprint arXiv:2002.02256*, 2020.
- [73] X. Jin, C. Lan, W. Zeng, and Z. Chen, “Uncertainty-aware multi-shot knowledge distillation for image-based object re-identification,” in *Proceedings of the AAAI Conference on Artificial Intelligence*, vol. 34, no. 07, 2020, pp. 11 165–11 172.
- [74] Y. Bai, Y. Lou, Y. Dai, J. Liu, Z. Chen, and L.-Y. Duan, “Disentangled feature learning network for vehicle re-identification,” in *International Joint Conferences on Artificial Intelligence*, 2020, pp. 474–480.
- [75] Y. Bai, Y. Lou, F. Gao, S. Wang, Y. Wu, and L.-Y. Duan, “Group-sensitive triplet embedding for vehicle reidentification,” *IEEE Transactions on Multimedia*, vol. 20, no. 9, pp. 2385–2399, 2018.
- [76] Y. Yuan, K. Yang, and C. Zhang, “Hard-aware deeply cascaded embedding,” in *International Conference on Computer Vision*, 2017, pp. 814–823.
- [77] F. Schroff, D. Kalenichenko, and J. Philbin, “Facenet: A unified embedding for face recognition and clustering,” in *Conference on Computer Vision and Pattern Recognition*, 2015, pp. 815–823.